

Voltage Improvement by a Transformerless Active Voltage Quality Regulator with the Parasitic Boost Circuit

Mahesh S. Khande¹, A K Jhala², Manish Prajapati³

PG Scholar, RKDF College of Engineering, Bhopal, India¹

Associate Professor, RKDF College of Engineering, Bhopal, India²

Assistant Professor, RKDF College of Engineering, Bhopal, India³

Abstract: Voltage sags have always been a more threat to sensitive industrial and commercial electrical consumers, and deep sags with long duration time are usually more intolerable. In this paper, a new study of series-connected compensator is presented to mitigate long duration deep sags, and the solatium ability is highly improved with an unrivalled shunt converter structure acting as a parasitic boost circuit that has been theoretically analyzed. Additionally, the projected active voltage quality regulator is a cost effective solution for long duration sags that are lower than 50% of the nominal voltage as it is transformerless compared with the traditional dynamic voltage restorer. High operation efficiency is ensured by applying the dc-link voltage adaptive control method. Analysis, along with simulation and experimental results, is presented to verify the feasibility and effectiveness of the projected study.

Keywords: Dynamic Voltage Restorer (DVR), Dynamic Sag Correction, Long Duration Deep Sag, Parasitic Boost Circuit, Series Connect Compensator.

I. INTRODUCTION

Power quality (PQ) problems have obtained increasing attentions as they can affect lots of sensitive end-users including industrial and commercial electrical consumers. Studies indicate that voltage sags, transients, and momentary interruptions constitute 92% of all the PQ problems occurring in the distribution power system [1]. In fact, voltage sags have always been a more threat to the industry, and even 0.25 s voltage sag is long enough to interrupt a manufacture process resulting in enormous financial losses [2], [3]. Voltage sags are generally classified according to its depth and duration time. Typical sag can be a drop to between 10% and 90% of the rated RMS voltage and has the duration time of 0.5 cycles to 1 min [4].

According to the data presented in [5], majority of the sags recorded are of depth no less than 50%, but larger sags with long duration time obviously cannot be ignored as they are more intolerable than shallow and short-duration sags to the sensitive electrical more characteristics about voltage sags are described in [6].

Many customer power devices have been projected to mitigate such voltage sags for sensitive loads [7]. The most studied voltage regulator topologies can generally categorized into two groups: the inverter based regulator and direct ac-ac converters. In [8]– [11], several ac-ac converter-based regulators are introduced. Series-connected devices (SD) are voltage-source inverter-based regulators and an SD compensate for voltage sags by injecting a missing voltage in series with the grid [12].

There are lots of SD topologies, and key features related to the evaluation of a certain SD study are the cost, complexity, and solatium ability. Dynamic voltage restorer (DVR) is a commonly used SD and has been widely studied. Different types of DVRs are discussed in [13]. In [14], four typical DVR system topologies are investigated and experimentally compared. The overall evaluation has shown that DVR with no storage and load-side-connected shunt converter ranks the highest as it can compensate for long-duration deep sags at a relatively low complexity and cost. Applications based on this study are given in [15]– [20].

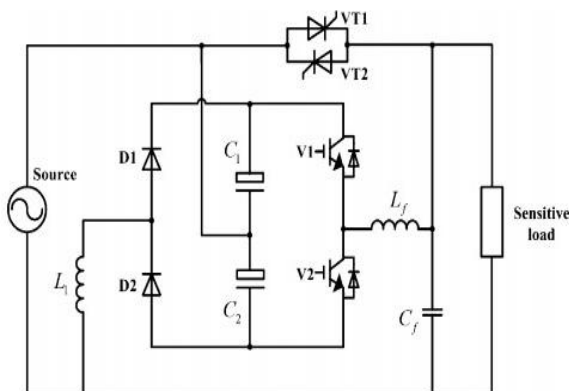


Fig. 1 Single-phase DySC configuration consumers

However, the aforementioned DVR study is still not a cost effective solution for long duration deep sags as it regularly contains a series transformer that is heavy, bulky, and costly operating at the line frequency [16]. This drawback is obviously non ignorable especially in low-power applications. In [21] and [22], a type of transformerless SD study known as dynamic sag corrector (DySC) is projected, and it is a low cost, small size, light weight, and highly effective system for sag mitigation as the series transformer is no longer needed. There are several circuit structures of the DySC including two given in [21] and [22], and Fig. 1 illustrates another possible configuration. When the grid voltage differs from its desired waveform, a missing voltage will be injected and filtered by the DySC through its half-bridge series converter (V1, V2) and output filter (L_f, C_f) to maintain the load voltage at its rated value. During this period of time, the energy needed for the solatium is provided by the residual supply via a passive shunt converter (D1, D2, L₁) and stored in the dc-link capacitors (C1, C2). So, the dc-link voltage should always be lower than the peak value of the supply voltage, and it means that the DySC can only compensate for voltage sags no larger than 50% since the largest injection voltage of the DySC is solely determined by its dc link voltage. As mentioned in [21] and [22], the ride through time of the DySC in larger voltage sags is limited by the dc-link energy storage, and it is inadequate to provide reliable protection for sensitive loads. So, although the DySC is an excellent solution for sags in many cases, it is invalid for long-duration deep sags as its solatium ability is limited by the passive rectifier. In [23] and [24], either PWM rectifier or backup grid is adopted to increase the energy provided during voltage sags. But the solatium ability is greatly enhanced at the expense of significantly increasing the complexity and cost. In this paper, position of the shunt converter and series converter in the DySC is changed according to the structure differences between the DVR with the load-side-connected shunt converter and the DVR with the supply-side-connected shunt converter. As a result, the shunt converter together with the series converter formed a boost charging circuit and the dc-link voltage will be charged to exceed the peak value of the supply voltage. This obtained novel study is called the transformerless active voltage quality regulator with the parasitic boost circuit (PB-AVQR), and it is capable of mitigating long duration deep voltage sags without increasing the cost, volume, and complexity compared with the traditional DySC study. The dc-link voltage adaptive control method projected in [25] is also applied in the PB-AVQR to improve its operation efficiency. This paper starts with introducing the operating mode and working principles of the projected configuration. Then, the parasitic boost circuit model is provided followed by the theoretical analysis to calculate its dc-link voltage. At last, the simulation results using MATLAB and experimental results on a 220 V-2 kW prototype are given to verify the feasibility and effectiveness of the PB-AVQR study.

II. STUDY AND PRINCIPLE

As shown in Fig. 2, the PB-AVQR study is mainly consists of five parts, including a static bypass switch (VT1, VT2), a half-bridge inverter (V1, V2), a shunt converter (VT3, VT4), a storage module (C1, C2), and a low-pass filter (L_f, C_f). The operating mode and applied control strategies are similar to what have been described in [25]. Under normal operating conditions, the static bypass switch is controlled to switch on and the normal grid voltage is delivered directly to the load side via this bypass switch. When an abnormal condition is detected, the static bypass switch will be switched OFF and the inverter will be controlled to inject a desired missing voltage in series with the supply voltage to ensure the power supply of sensitive loads. There are totally two different kinds of control strategies

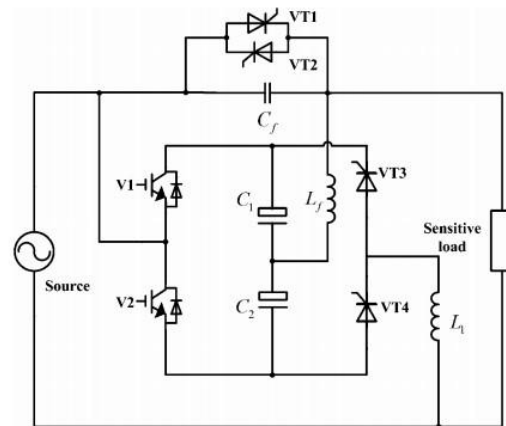


Fig. 2. Projected PB-AVQR study.

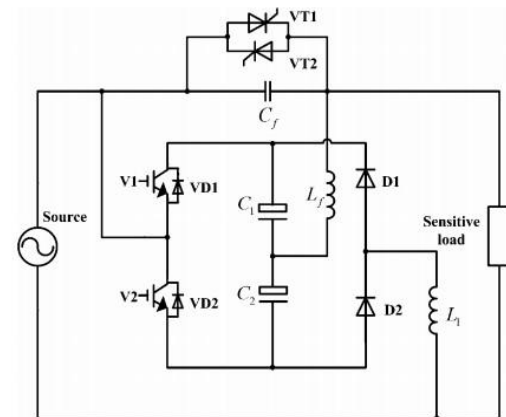


Fig. 3. SPB-AVQR study

in the projected PB-AVQR system. When the grid voltage is lower than the rated voltage, an in-phase control strategy will be adopted and a phase-shift control strategy will be applied when the supply voltage is higher than the nominal voltage. Working principle of the PB-AVQR is different compared with that of the DySC due to its unrivalled shunt converter structure. When the projected configuration is analyzed, both the operating states of the

switches (V1, V2) and the trigger angles of the thyristors (VT1, VT2) should be taken into consideration. So, a simplified PB-AVQR (SPB-AVQR) circuit shown in Fig. 3, where two thyristors (VT3, VT4) in the projected PB-AVQR are replaced by two diodes (D1, D2), is firstly introduced to better explain its working principles. The following analysis will be based on the SPB-AVQR which can be regarded as a special type of PB-AVQR. The only difference between these two configurations is that the shunt converter of the PB-AVQR is controllable while the shunt converter of the SPB-AVQR is uncontrollable. That is to say, the dc-link voltage of the SPBAVQR represents the upper limit of the dc-link voltage in the PB-AVQR structure. So, theoretical conclusions drawn with the SPB-AVQR are basically applicable to the PB-AVQR.

As shown in Fig. 3, switches V1 and V2 are now also parts of the parallel circuit, which means that the dc-link voltage will be affected by the on/off status of the switches. So, the turn on and turn off conditions of the solatium process should be considered to understand the working principles circuit of the SPB-AVQR. Figs. 4 and 5 about the parasitic boost

illustrate four different operating conditions of the SPB-AVQR within ones witching cycle during the positive and negative half-cycle of the sinusoidal supply voltage separately. Both the solatium process and charging process can be explained based on these operating conditions. In Figs. 4 and 5, the solid line means that there is current flowing through and arrows depict directions.

Operating conditions during the positive half-cycle are illustrated in Fig. 4. When V2 is switched on, as shown in Fig. 4(a), the grid charges the inductor L1 via the diode D2 and the capacitor C2 discharges to maintain the load voltage. When V2 is switched off, as shown in Fig. 4(b), the energy stored in the inductor during previous period is released to dc-link capacitors C1 and C2 through VD1 which is the antiparallel diode of V1. Operating conditions during the negative half-cycle are given in Fig. 5. When V1 is switched on, as shown in Fig. 5(a), the inductor L1 is charged via the diode D1, and the load is compensated by the capacitor C1. When V1 is switched off, as shown in Fig. 5(b), the energy stored in L1 is released through VD2, which is the antiparallel diode of V2, to capacitors C1 and C2. So, in each half-cycle of the grid, one capacitor of the dc-link discharges to provide the energy needed for the solatium, and this energy is actually obtained from the supply source via the charging process described earlier

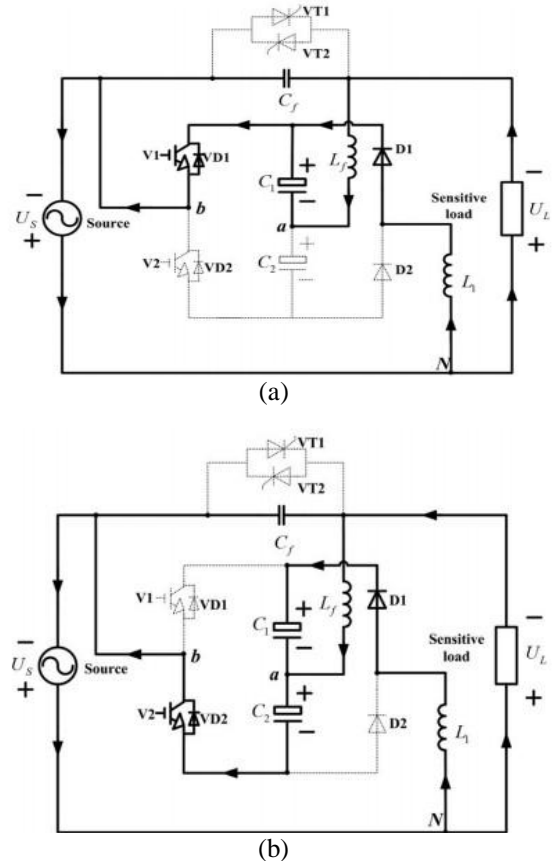
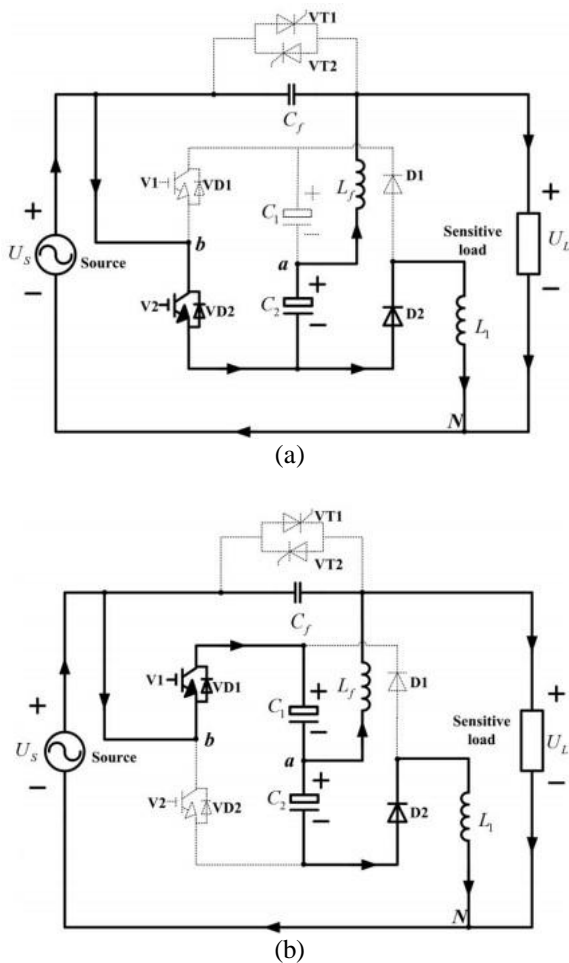


Fig. 4. Operating conditions during positive halfcycle. (a) V2 switched on.(b) V2 switched off.

Fig. 5. Operating conditions during negative half-cycle. (a) V1 switched on. (b) V1 switched off.

Apparently, the charging circuit of the projected configuration works exactly like a boost circuit and the dc-link voltage in this situation is controlled by the duty ratio of the two switches. So, the solatium ability of the SPB-AVQR is theoretically unlimited as long as the grid is strong enough to provide the needed power. However, as the boost circuit is parasitic on the series inverter, and the two switches are actually controlled according to the missing voltage, there still exist some restrictions. The relationships between the dc-link voltage and other system parameters will be discussed in the next section.

In Figs. 4 and 5, two endpoints of the inverter are marked as a and b. Parts of the waveforms obtained at the inverter side and load side under four operating conditions are schematically shown in Fig. 6, where U_{aN} represents the voltage between a and N. As shown in Fig. 6, when V1/V2 is switched on/off, the dc-link voltage will be added/subtracted to the supply voltage to get a switching pulse voltage U_{aN} and the switching harmonics of U_{aN} will be filtered by L_f and C_f to get a smooth load voltage. So, the load voltage will be maintained at its rated value if the inverter is properly controlled according to the required missing voltage during sags.

III. MODELING AND THEORETICAL ANALYSIS

DC-link voltage is a key parameter to evaluate the solatium ability about a series solatium device since it decides

the maximum value of the injected solatium voltage. In this section, in order to evaluate the solatium ability of the projected study and verify its feasibility in mitigating long duration deep sags, relationships between the dc-link voltage and other system parameters will be derived based on the circuit model of the aforementioned operating conditions. As can be seen from Figs. 4 and 5, working principles during the positive and negative half-cycle of the supply voltage are the same, so the following analysis will be focused on the situation in the positive half-cycle. The control strategy applied for voltage sags is in-phase solatium, so the energy needed to maintain the load voltage in one half-cycle can be expressed as follows [26]:

$$E_0 = \frac{T_0 \Delta V}{2V_{ref}} P_0 \tag{1}$$

where T_0 is the grid voltage period time, V_{ref} is the rated rms value of the load voltage, P_0 is the rated load power, and ΔV is the rms value of the missing voltage. In steady-state solatium, the energy needed for the solatium should completely be provided by the residential grid which is also the charging energy through the parasitic boost circuit in this case. So the charging energy provided during $T_0/2$ referred to as E_1 equals to E_0 . E_0 can be easily obtained according to (1), but the calculation of E_1 involves with the operating conditions shown in Fig. 4. The simplified circuit model of Fig. 4 is illustrated in Fig. 7, where solatium loop including the filter and the load is ignored and only the charging circuit is considered

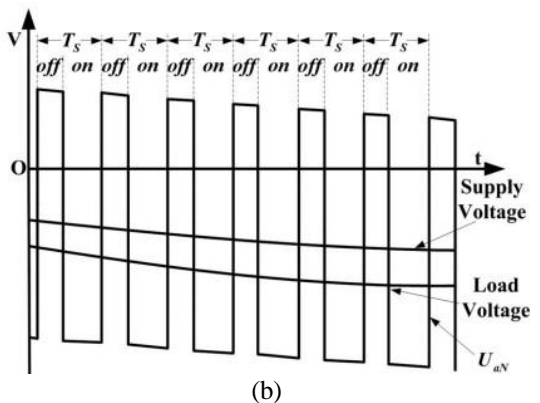
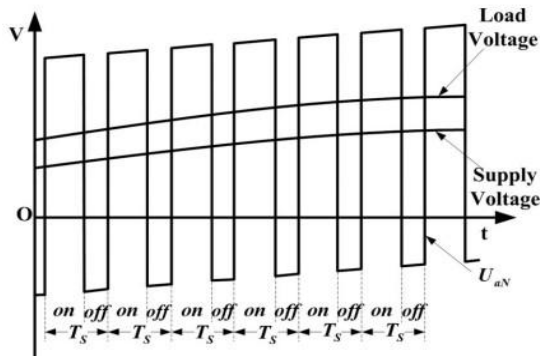


Fig. 6. Waveforms of supply voltage, load voltage, and U_{aN} . (a) V2 on/off. (b) V1 on/off.

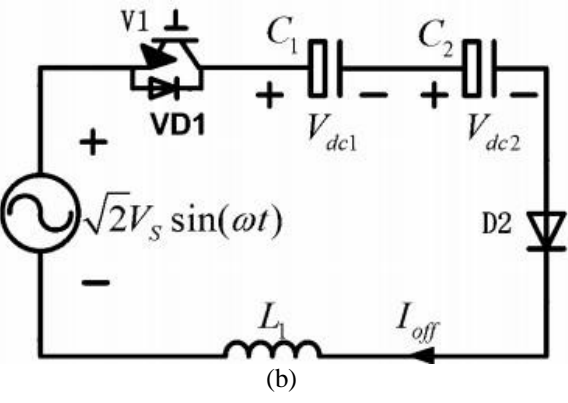
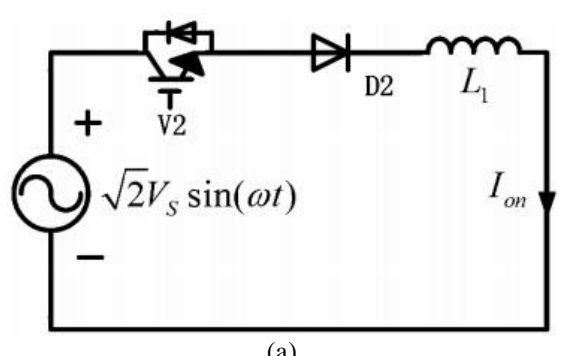


Fig. 7. Simplified circuit model. (a) V2 turned on. (b) V2 turned off

In Fig. 7, VS is the rms value of the supply voltage. Two state equations can be obtained based on Fig. 7 and written as follows:

$$L1 \frac{dI_{on}}{dt} = \sqrt{2} V_s \sin(\omega t)$$

$$\frac{dI_{off}}{dt} = \sqrt{2} V_s \sin(\omega t) - V_{dc1} - V_{dc2} \quad (2)$$

According to [27] and [28], the analysis will be significantly simplified if some realistic approximations are carried out. Then(2) can be discretized into (3) based on two following assumptions: C1 and C2 are well designed so that Vdc1 and Vdc2 can be regarded equal without considering their ripple voltages; the switching frequency is much higher than the line frequency that the supply voltage in the nth switching cycle can be treated as a constant value

$$L1 \Delta I_{onn} = \sqrt{2} V_s \sin(\omega n T_s)$$

$$L1 \Delta I_{offn} = [\sqrt{2} V_s \sin(\omega n T_s) - 2V_{dc}] t_{offn} \quad (3)$$

where tonn and toffn are, respectively, the turn-on and turn-off time of V2 in the nth switching cycle, Ts is the switching period, Vdc is the steady-state dc-link voltage, and ΔIonn or ΔIoffn represents the variation amount in charging current during ton or toffn . As the analysis is within the positive half-cycle of the grid, there exists a constraint: $n \leq T_0 / 2T_s$. Apparently, tonnand toffn here are actually the inverter’s duty cycle and they canbe expressed as (4) when two-level symmetric regular-sampled

PWM method is adopted [29]

$$t_{onn} = \frac{T_s}{2} \left[1 + \frac{\sqrt{2} \Delta V_s \sin(\omega n T_s)}{V_{dc}} \right]$$

$$t_{offn} = \frac{T_s}{2} \left[1 - \frac{\sqrt{2} \Delta V_s \sin(\omega n T_s)}{V_{dc}} \right] \quad (4)$$

The recursion formula of the charging current at the end of the nth switching cycle can be obtained by combining (3) and(4)

$$I_{offn} = I_{offn(n-1)} + \frac{T_s}{L1} [\sqrt{2} V_{ref} \sin(\omega n T_s) - V_{dc}] \quad (5)$$

where Ioffn represents the charging current instantaneous value at the end of the nth switching cycle and ΔIonn can be derived at the same time

$$\Delta I_{onn} = \frac{\sqrt{2} \Delta V_{ref} \sin(\omega n T_s)}{2L1} \left[1 + \frac{\sqrt{2} \Delta V_s \sin(\omega n T_s)}{V_{dc}} \right] \quad (6)$$

The energy stored in an inductor is related to the current that flows through it, so the charging energy provided by the grid via the parasitic boost circuit in the nth switching cycle can be expressed and then rearranged as follows:

$$E_{inn} = \frac{1}{2} L1 \Delta I_{onn}^2 + L1 I_{offn(n-1)} \Delta I_{onn} \quad (7)$$

Ioff (n – 1) in (7) can be superimposed according to the recursion formula shown in (5). Before the expression is given, there are some features about the charging current should be clarified: 1) the value of the charging current cannot be lower than zero as the current flowing through a diode is unidirectional; 2) the value of the charging current can either be zero or non zero and its value always decreases after increasing in one half-cycle of the sinusoidal grid voltage. Then, the nonzero terms of the charging current can be derived as follows:

$$I_{off(n-1)} = \sum_{k=n_0}^{n-1} \frac{T_s}{L1} [\sqrt{2} V_{ref} \sin(\omega k T_s) - V_{dc}] \quad (8)$$

where n0 is the initial superposition instant and Ioffn is always equal to zero when n is smaller than n0 . So, n0 can be calculated according to (5) and expressed as follows:

$$n_0 = \text{ceil} \left(\frac{T_0 \arcsin \frac{V_{dc}}{V_{ref}}}{2\pi T_s} \right) \quad (9)$$

where ceil(•) represents the rounded up function and the arcsine function here ranges from 0 to π/2. Furthermore, when the charging current calculated by (8) decreases to the value no more than zero, n will reach its upper limit denoted by ne .Substituting (6), (8), and (9) into (7), the energy provided by the supply in the nth switching cycle can be written as follows:

$$E_{inn} = \frac{T_s^2 V_s^2 A^2}{4 L1} (1 + \sqrt{2} B A)^2 + \frac{\sqrt{2} T_s^2 V_s A}{2 L1 V_{dc}} (V_{dc} + \sqrt{2} \Delta V_A) \sum_{k=n_0}^{n-1} [\sqrt{2} V_{ref} C - V_{dc}] \quad (10)$$

Where

$$A = \sin(\omega n T_s)$$

$$B = \frac{\Delta V}{V_{dc}}$$

$$C = \sin(\omega k T_s)$$

E1 now can be obtained if (10) is added with n ranging from 1 to T0 / 2Ts . So, the overall energy balance equation can be written as follows:

$$E1 = \frac{T_s^2 V_s^2}{4 L1} \left(\sum_{n=1}^{\frac{T_0}{2T_s}} A^2 + \sqrt{2} B \sum_{n=1}^{\frac{T_0}{2T_s}} A^3 + 2B \sum_{n=1}^{\frac{T_0}{2T_s}} A^4 \right) + \frac{T_s^2 V_s^2 A^2}{4 L1} \sum_{n=n_0}^{n_e} [(A + \sqrt{2} B A^2) \sum_{k=n_0}^{n-1} [\sqrt{2} V_{ref} C - V_{dc}]] = T_0 \Delta V_2 V_{ref} P_0 = E_0 \quad (11)$$

The charging current peak value Imax is considered to arise at the switching cycle after the value of (8) reaches its upper limit. So Imax is expressed as follows:

$$I_{max} = \frac{\sqrt{2} T_s V_s \sin(\omega n_{max} T_s)}{2 L1} [1 + \sqrt{2} B \sin(\omega n_{max} T_s)] + \sum_{k=n_0}^{n_{max}} \frac{T_s}{L1} [\sqrt{2} V_{ref} C - V_{dc}] \quad (12)$$

where nmax is the switching cycle when Ioffn reaches its maximum value and nmax can be written as follows:

$$n_{max} = \text{ceil} \left[\frac{T_o(\pi - \arcsin \frac{V_{dc}}{V_{ref}})}{2\pi T_s} \right] \quad (13)$$

So far, the main features of the SPB-AVQR study can be described by (11) and (12). As shown in (11), the dc-link voltage is not only related to the supply voltage, but also associated with the charging inductance, load active power, and switching frequency. However, the dc-link voltage cannot be obtained directly from (11) as n_0 and n_e cannot be computed with unknown dc-link voltage. So, an iterative algorithm is applied to estimate the dc-link voltage, where $T_s, V_s, T_0, V_{ref}, L_1$, and P_0 are all treated as constants. A flow chart of the adopted calculating method is illustrated in Fig. 8, where V_{dc0} is the initial value for V_{dc} and ΔV_{dc} is the iterative step. The algorithm is terminated if the error between E_0 and E_1 is smaller than the error tolerance ϵ . Moreover, the charging current can be calculated by (12) and (13) as long as V_{dc} is obtained. Fig. 9 shows the relationships between the steady state dc link voltage and the supply voltage with different inductance values obtained according to (11). Other system parameters are listed as

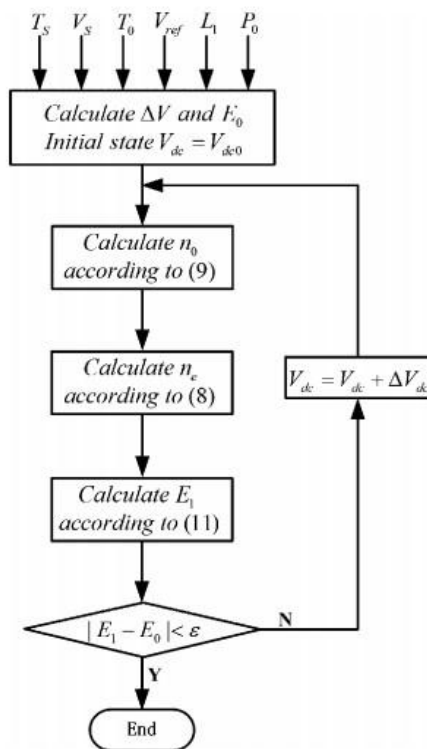


Fig. 8. Flow chart for calculating V_{dc}

follows: $P_0 = 2 \text{ kW}$, $T_s = (1/15000)\text{s}$, $T_0 = 0.02 \text{ s}$, $V_{ref} = 220 \text{ V}$. The black solid line in Fig. 9 is the V_{dc} - V_s curve of the DySC study. As can be seen in Fig. 9, the steady-state dclink voltage of the SPBAVQR under different supply voltage is much higher than that of the DySC study and it decreases slightly with the falling of the supply. Additionally, when the supply voltage is lower than 50% of its rated value, the dc-link voltage of the SPB-AVQR is

still maintained high enough for the solatium while that of the DySC is too low to mitigating the deep sag. Fig. 9 also indicates that the dc-link voltage of the SPB-AVQR becomes higher with a lower inductance under the same circumstance. Fig. 10 gives the I_{max} - V_s curve under the same condition.

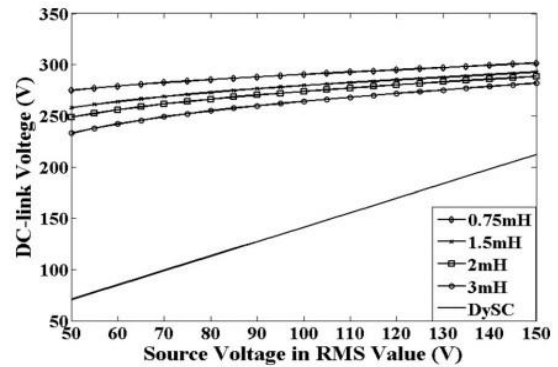


Fig. 9. V_{dc} - V_s curve of the SPB-AVQR with different inductances.

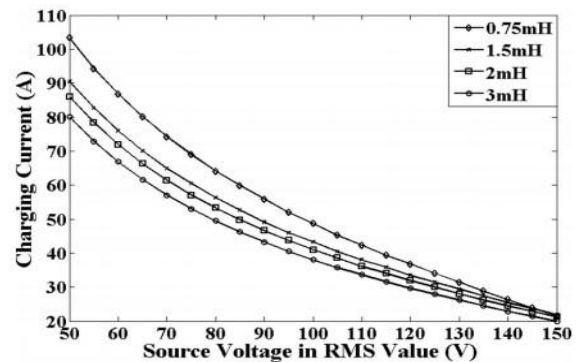


Fig. 10. I_{max} - V_s curve of the SPB-AVQR with different inductances.

It presents that the steady-state charging current peak value increases with the decreasing of the supply voltage and it can be suppressed by increasing the charging inductance. Although conclusions drawn from the theoretical analysis for the SPB-AVQR can also be applied to the projected PB-AVQR study, there still exist some differences in their dc-link voltages.

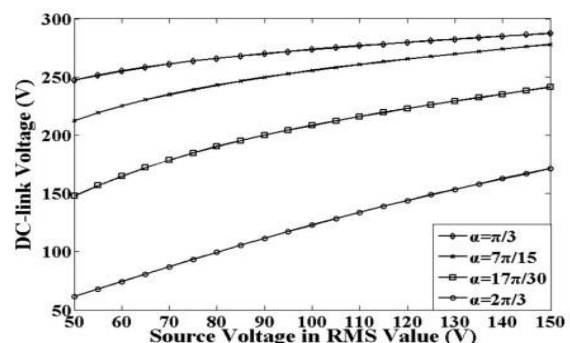


Fig. 11. V_{dc} - V_s curve of the PB-AVQR with different trigger angles. projected

When the PB-AVQR is discussed, the trigger pulse angle α for VT3 and VT4 should also be taken into consideration. In the PB-AVQR circuit, the charging process begins after the VT3 or VT4 is triggered, so the initial superposition instant n_0 in (11) is now determined by α denoted by n_1 and the energy balance equation is written as follows:

$$\frac{T_s^2 V_s^2}{4 L_1} \left(\sum_{n=n_1}^{n_e} A^2 + 2 \sqrt{2} B \sum_{n=n_1}^{n_e} A^3 + 2 B^2 \sum_{n=n_1}^{n_e} A^4 \right) + \frac{T_s^2 \sqrt{2} V_s}{2 L_1} \sum_{n=n_1}^{n_e} [(A + \sqrt{2} B A^2) \sum_{k=n_1}^{n-1} [\sqrt{2} V_{ref} C - V_{dc}]] = T_o \Delta V_2 V_{ref} P_o \quad (14)$$

Here, n_e is still determined by (8) as aforementioned and n_1 can be derived as follows:

$$n_1 = \text{ceil} \left[\frac{\alpha T_o}{2\pi T_s} \right] \quad (15)$$

Furthermore, the thyristors are triggered only once in each half-cycle and the current through them should be higher than the holding current to maintain the triggered state. So, α is required to meet the constraint expressed as follows:

$$\sqrt{2} V_{ref} \sin \alpha > V_{dc} \quad (16)$$

The charging current peak value of the PB-AVQR can still be described by (12) as long as n_0 is substituted with n_1 . As can be seen from (14) and (15), the trigger pulse of the PB-AVQR will certainly affect its dc-link voltage and charging current. Fig. 11 shows the $V_{dc} - V_s$ curve under the influence of α according to (14). The charging inductor in Fig. 11

is set to 2 mH and other parameters remain the same as those in Fig. 9. Fig. 11 demonstrates that the steady-state dc-link voltage gets higher with a smaller trigger angle as the charging time becomes longer. It also indicates that the PB-AVQR is capable of mitigating deep sags with a proper trigger pulse.

Fig. 12 present show α affects the $I_{max} - V_s$ curve under the same condition. As shown in Fig. 12, the charging current peak value can be reduced by decreasing α with the same supply voltage.

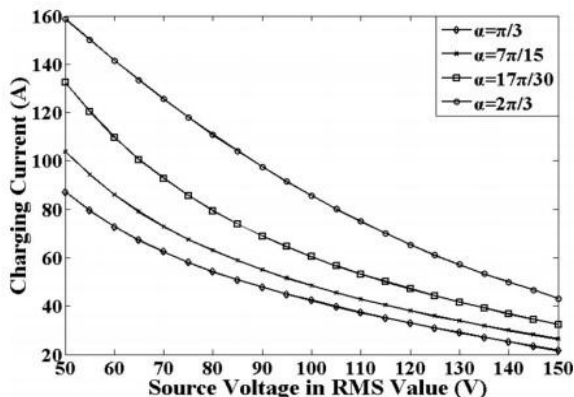


Fig. 12. $I_{max} - V_s$ curve of the PB-AVQR with different trigger angles.

IV. SIMULATION RESULTS

In order to show the validity of the projected PBAVQR, simulation and experimental results are presented in this section. The simulation results are based on the MATLAB software and the experimental results are based on a 2 kW single-phase prototype. The control method applied for the inverter is projected in [30] and the control method for the thyristors is demonstrated in [25].

A. System Parameters

There are mainly four parameters need to be designed, namely the dc-link capacitor $C1 / C2$, the filter inductor L_f , the filter capacitor C_f , and the charging inductor L_1 . During the steady-state solatium, one capacitor discharges at the switched-on position and two capacitors are both charged at the switched-off position in each switching cycle. Furthermore, $C1$ and $C2$ discharge, respectively, in the negative and positive half-cycle of the supply. So, if the two capacitors are treated equally during the charging process, the energy-balance equation that required for the capacitors can be written as

$$\frac{T_o \Delta V}{4 V_{ref}} P_o = \frac{1}{2} C_1(2) V_{dc}^2 - \frac{1}{2} C_1(2) (V_{dc} - v_{dc})^2 \quad (17)$$

where v_{dc} is the fluctuation voltage of V_{dc} . In the theoretical analysis, the dc-link voltage is assumed to be a constant, so v_{dc}/V_{dc} here is limited within 5% at the voltage drop of 50% to minimize the overall dc link voltage ripple. In this way, the estimated minimum value of $C1 / C2$ can be calculated according to (17) with V_{dc} substituted by the dc-link set value V_{dc-set} . How to set the dc-link value is introduced in [25] and in this paper it is given as

$$V_{dc-set} = \begin{cases} 1.2 \times \sqrt{2} (V_{ref} - V_s) + 40 V_s < V_{ref} \\ 1.2 \times \sqrt{2} (V_s^2 - V_{ref}^2) + 40 V_s > V_{ref} \end{cases} \quad (18)$$

TABLE 1. SYSTEM PARAMETERS

| Description | parameters | Real value |
|---------------------|------------|------------|
| Nominal voltage | | 220V |
| Line frequency | | 50Hz |
| Switching Frequency | | 15KHz |
| DC-link capacitor | / | 4700uf |
| Filter inductor | | 1.5mH |
| Filter capacitor | | 20uF |
| Charging inductor | | 2mH |

As shown in Figs. 9–12, a higher dc-link voltage will be obtained with a smaller L_1 , but the peak value of the charging current will get larger at the same time. So, charging inductance L_1 is designed as a result of the compromise between the solatium ability and the charging current peak value.

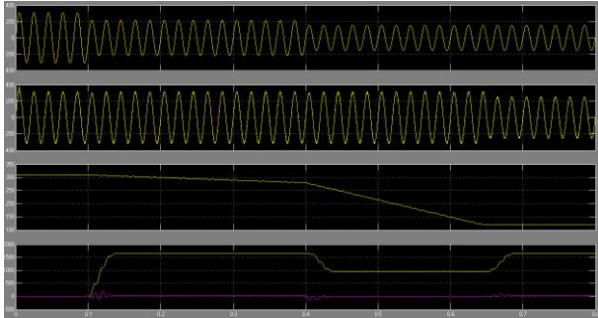


Fig. 13. Simulation result of the DySC.

The main function of the output LC filter in the projected structure is to eliminate the harmonic components of the injected solatium voltage. The value of Lf and Cf are designed according to its natural frequency and several other criterions which are given as follows [31]:

$$\frac{1}{2\pi\sqrt{L_f C_f}} = X_{fs} L_f < \frac{V_L}{\omega_{00} I_{L \max}} \quad (19)$$

$$C_f < \frac{I_{\text{ripple}} (\chi^2 + 1)}{8V_{dc} f_s}$$

where fs is the switching frequency, vL is the voltage drop across the inductor Lf at IL max, IL max is the maximum value of the load current, Iripple is the maximum ripple current of the filter and χ is the coefficient between the switching frequency and the filter’s natural frequency. Generally, χ ranges from 0.05 to 0.2. The PB-AVQR system’s key parameters are listed in Table 1 according to the design principles mentioned earlier.

B. Simulation Results

Fig. 13 shows the simulation results of the DySC study with different supply voltages. In the simulation, the supply

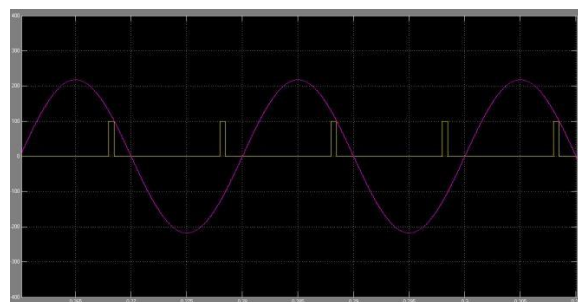


Fig. 14. Simulation result of the PB-AVQR.

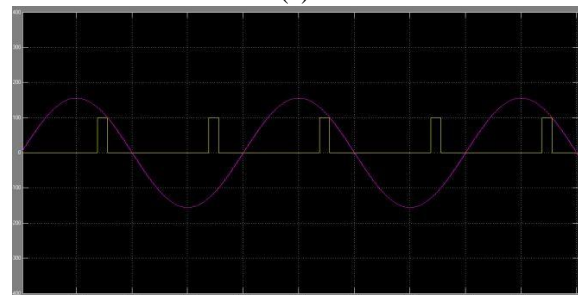
voltage drops to 180 V at 0.1 s and then falls to 100 V at 0.4 s. As shown in Fig. 13, when the supply voltage is 180 V, the DySC can effectively compensate for the voltage sag; however, when the supply voltage drops to 100 V, the load voltage becomes not sinusoidal as the maximum injected solatium voltage is limited by the low steady state dc-link voltage. Fig. 13 also indicates that the DySC can only mitigate deep sags for a few line cycles depending on the energy stored in dc-link capacitors as its steady-state

dc-link voltage is always lower than the peak value of the supply voltage. The graphics of the active and reactive power are also included in Fig. 13. When the supply voltage is 180 V, the dc-link voltage does not reach its steady state value with limited simulation time, so the active power of the supply is lower than the load power and its value is about 1.6 kW. When the dc-link voltage reaches its steady-state value with 100 V supply voltage, the active power of the supply is about 1.65 kW which means that the load voltage is no longer maintained. The simulation results of the projected PB-AVQR study under the same condition is shown in Fig. 14. As can be seen in Fig. 14, when supply voltage changes, the dc-link voltage precisely tracks Vdc-set according to (18) and it also remains enough high for the solatium even with a 100 V supply voltage. Fig. 14 also indicates that the transient response here is not very good, but this can be improved by increasing the set value for dc-link voltage. The active power of the supply during the steady-state solatium is 2 kW, and it is the same as the load power which means that the load voltage is effectively ensured. The reactive power during the steady-state solatium is about 1.1 kvar with 180 V supply and is about 1.4 kvar with 100 V supply. The reactive power of the projected PB-AVQR is higher than that of the DySC due to the dc-link voltage adaptive control method. Additionally, the instantaneous value of the active and reactive power can be suppressed by properly designing Vdc set and the charging time of the capacitors. Fig. 15 shows trigger pulses for thyristors under different grid voltage. The supply voltage is 180 V in Fig. 15(a) and is 100 V in Fig. 15(b).

As shown in Fig. 15, the trigger angle becomes smaller to ensure the solatium energy needed when the grid voltage decreases.



(a)



(b)

Fig. 15. Trigger signals under different supply voltage values. (a) 180 V supply voltage. (b) 100 V supply voltage.

V. CONCLUSION

This paper has presented a novel transformerless active voltage quality regulator with parasitic boost circuit to mitigate long duration deep voltage sags. The projected PB-AVQR study is derived from the DySC circuit and the solatium performance is highly improved without increasing the cost, weight, volume, and complexity. It is a relatively cost-effective solution for deep sags with long duration time compared with the traditional DVR study with load-side-connected shunt converter as a series transformer is no longer needed. The working principle and circuit equations are given through theoretical analysis.

Simulation and experimental results are presented to verify the feasibility and effectiveness of the projected study in the solatium for long duration deep voltage sags that are lower than half of its rated value. The operating efficiency of the projected PB-AVQR system also remains at a relatively high level as the dc-link voltage adaptive control method is adopted. In a conclusion, the projected PB-AVQR study in this paper provides a novel solution for long duration deep voltage sags with great reliability and solatium performance.

REFERENCES

- [1] Y. H. Chen, C. Y. Lin, J. M. Chen, and P. T. Cheng, "An inrush mitigation technique of load transformers for the series voltage sag compensator," *IEEE Trans. Power Electron.*, vol. 25, no. 8, pp. 2211–2221, Aug. 2010.
- [2] M. F. McGranaghan, D. R. Mueller, and M. J. Samotyj, "Voltage sags in industrial systems," *IEEE Trans. Ind. Appl.*, vol. 29, no. 2, pp. 397–403, Mar./Apr. 1993.
- [3] Bendre, D. Divan, W. Kranz, and W. Brumsickle, "Equipment failures caused by power quality disturbances," in *Proc. IEEE IAS Conf. Record*, 2004, pp. 482–489.
- [4] M. F. Alves and T. N. Ribeiro, "Voltage sag: an overview of IEC and IEEE standards and application criteria," in *Proc. IEEE Transmiss. Distrib. Conf.*, 1999, vol. 2, pp. 585–589.
- [5] S. Subramanian and M. K. Mishra, "Interphase AC–AC study for voltage sag supporter," *IEEE Trans. Power Electron.*, vol. 25, no. 2, pp. 514–518, Feb. 2010.
- [6] M. H. J. Bollen, *Understanding Power Quality Problems, Voltage Sags and Interruptions*. Piscataway, NJ, USA: IEEE Press, 2002.
- [7] Sannino, M. G. Miller, and M. H. J. Bollen, "Overview of voltage sag mitigation," in *Proc. IEEE Power Eng. Soc. Winter Meet.*, 2000, vol. 4, pp. 2872–2878.
- [8] S. M. Hietpas and M. Naden, "Automatic voltage regulator using an AC voltage-voltage converter," *IEEE Trans. Ind. Appl.*, vol. 36, no. 1, pp. 33–38, Jan./Feb. 2000.
- [9] Z. Fedyczak, R. Strzelecki, and G. Benysek, "Single-phase PWM AC/AC semiconductor transformer topologies and applications," in *Proc. 33rd Annu. IEEE Power Electron. Spec. Conf.*, Jun. 2002, pp. 1048–1053.
- [10] J. Hoyo, J. Alcalá, and H. Calleja, "A high quality output AC/AC cuk converter," in *Proc. 35th Annu. IEEE Power Electron. Spec. Conf.*, 2004, pp. 2888–2893.
- [11] J. Hoyo, H. Calleja, and J. Arau, "Three-Phase PWM AC/AC cuk converter for voltage sag solatium," in *Proc. 37th IEEE Power Electron. Spec. Conf.*, 2006, pp. 1–5.
- [12] S. W. Middlekauff and E. R. Collins, "System and customer impact: Considerations for series custom power devices," *IEEE Trans. Power Del.*, vol. 13, no. 1, pp. 278–282, Feb. 1998.
- [13] J. Praveen, P. Bishnu, M. S. Venkateshwarlu, and H. V. Makthal, "Review of dynamic voltage restorer for power quality improvement," in *Proc. 30th Annu. IEEE Ind. Electron. Soc.*, 2004, pp. 749–752.
- [14] J. G. Nielsen and F. Blaabjerg, "A detailed comparison of system topologies for dynamic voltage restorers," *IEEE Trans. Ind. Appl.*, vol. 41, no. 5, pp. 1272–1280, Sep./Oct. 2005.